International Journal of
Organizational Innovation

IDENTIFICATION OF SHEAR BANDS USING MICROTREMOR MEASUREMENT RESULTS

Tse-Shan Hsu
President, Institute of Mitigation for Earthquake Shear Banding Disasters
Professor, Feng-Chia University, Taiwan, R.O.C., tshsu@fcu.edu.tw

Hsin-Mao Wang
Ph.D. Student, Ph.D. Program for Infrastructure Planning and Engineering
Feng-Chia University, Taiwan, R.O.C.

Tsai-Fu Chuang
Associate Professors, Feng-Chia University, Taiwan, R.O.C.

Abstract

Shear bands pose a significant threat to structural safety; therefore, their early detection is crucial when selecting sites for building construction. Existing literature primarily describes qualitative approaches to shear band identification, utilizing satellite imagery and field photographs in conjunction with topographic features indicative of displacement along shear bands. To address the need for a quantitative identification method, this study conducted in-situ micro-vibration measurements at sites of building collapse during the 1999 Jiji earthquake. Based on the micro-vibration analysis results, a novel quantitative approach for identification shear bands is proposed. The effectiveness and accuracy of this method are further validated by comparing its results with the actual locations of shear bands in the field.

Keywords: shear bands, identification, micro-vibration, structural safety.

Introduction

Micro-vibration measurements were conducted at eight locations around the collapsed school building at Guangfu Junior High School in Wufeng, Taichung, as shown in Figure 1. The measurements were performed using the pALERT Q332 instrument (Figure 2), which recorded acceleration time-series data in the vertical and two mutually perpendicular horizontal directions. These data were then analyzed to extract spectral information for all three components. The analysis results are presented below.

(a) Facing the internal campus

(b) Facing the external campus

(c) Actual location of the sixth measurement point

Figure 1. Distribution of Micro-Vibration Measurement Points in the Vicinity of the Collapsed Building (Google Earth, 2023).

Figure 2. Micro-vibration measuring system consisting of a pALERT Q332 instrument and a computer.

Time History Curves and Spectral Characteristics of Microtremors

The micro-vibration measurement technique adopted in this study (Wen, 2023) involves recording acceleration time histories in the vertical and two orthogonal horizontal directions. These time-series data enable spectral analysis in all three components.

Figures 3 through 10 display the ground microtremor acceleration time histories recorded at Monitoring Points 1 through 8, respectively, in the vertical, horizontal-1, and horizontal-2 directions. For each case, the corresponding frequency-domain spectra, derived using the Fast Fourier Transform (FFT), are also presented.

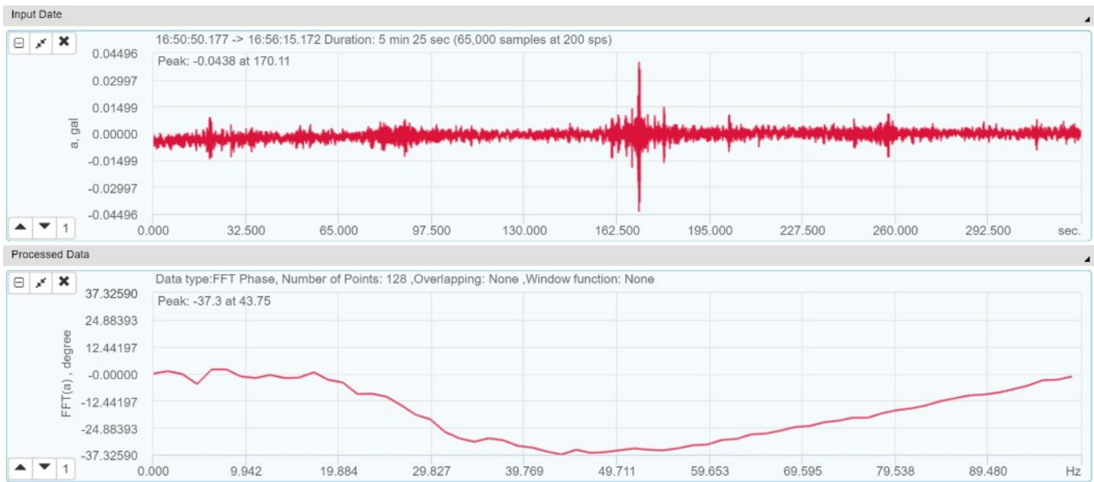

(a) Vertical direction

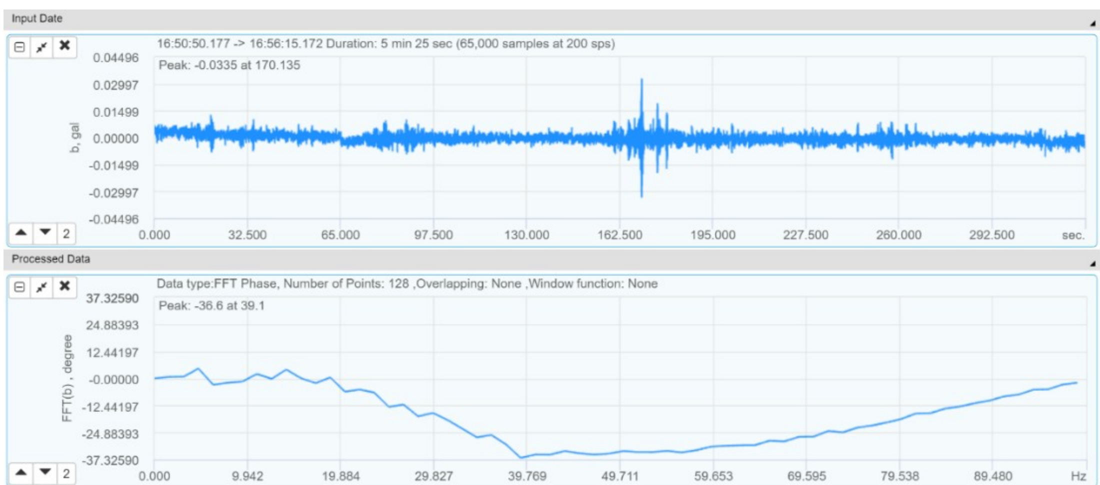

(b) Horizontal direction 1

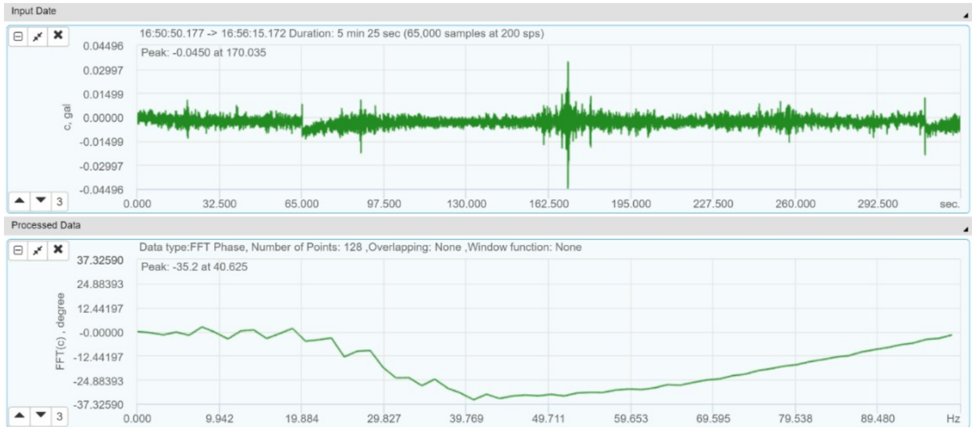

(c) Horizontal direction 2

Figure 3. Three-Component Micro-Vibration Time Histories and Corresponding Frequency Spectra at Monitoring Point 1.

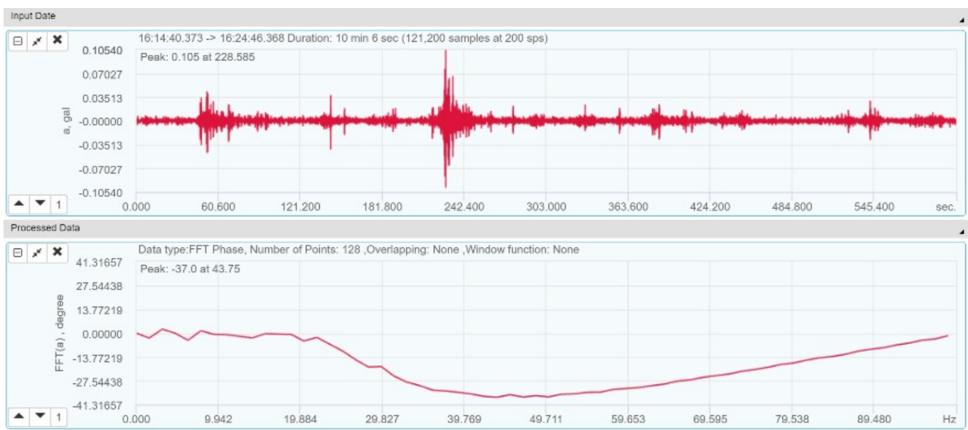

(a) Vertical direction

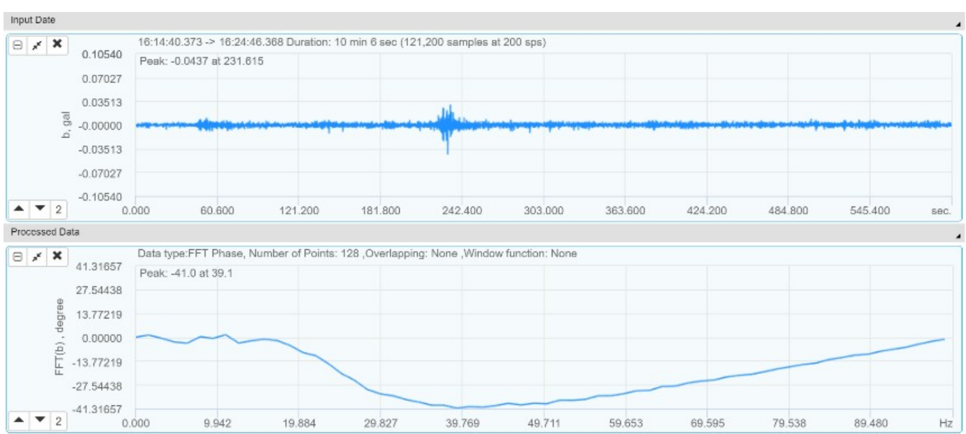

(b) Horizontal direction 1

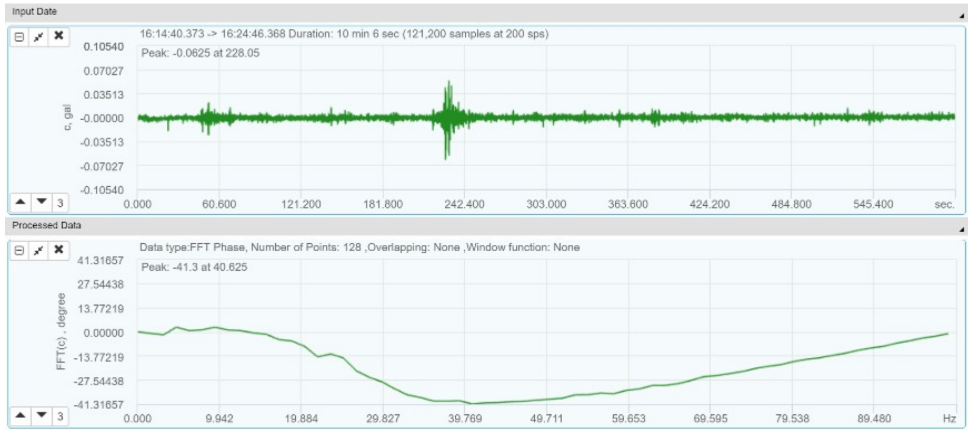

(c) Horizontal direction 2

Figure 4. Three-Component Micro-Vibration Time Histories and Corresponding Frequency Spectra at Monitoring Point 2.

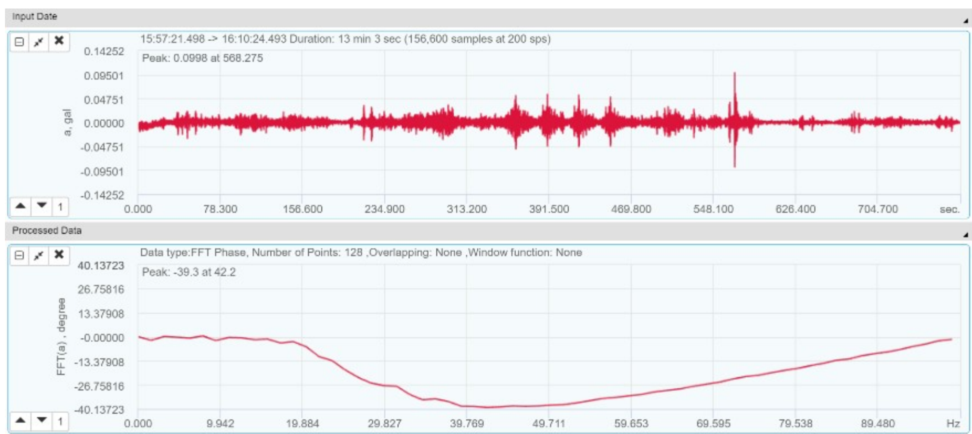

(a) Vertical direction

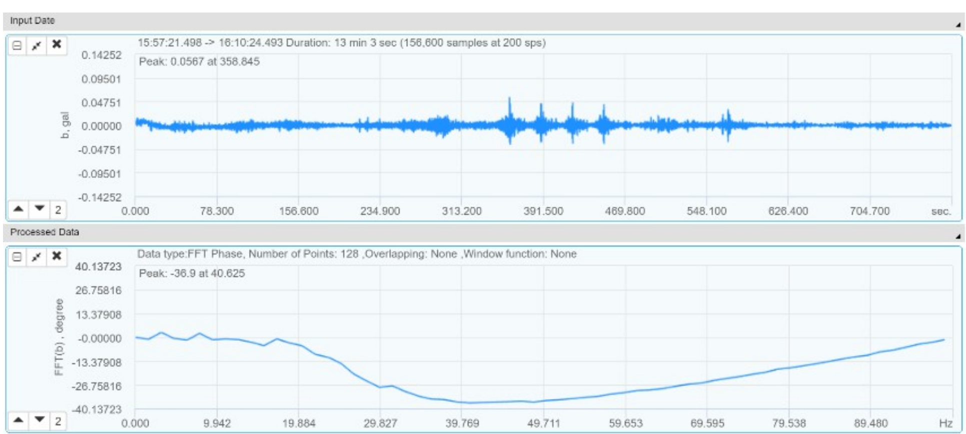

(b) Horizontal direction 1

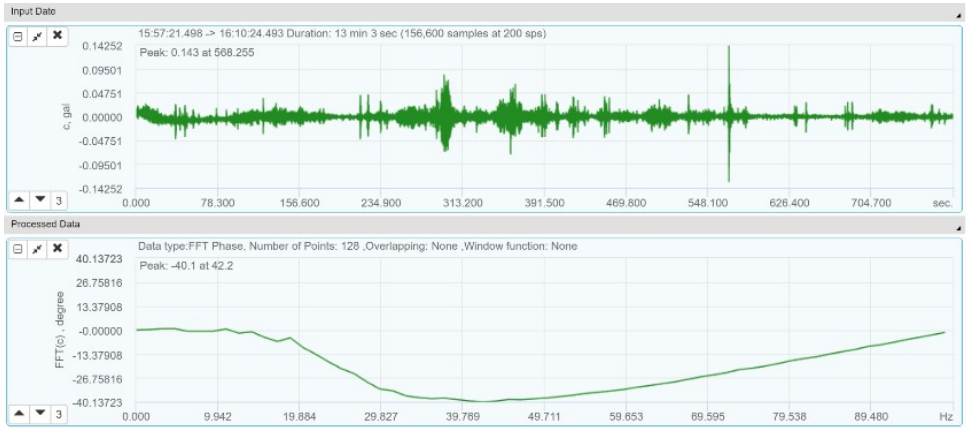

(c) Horizontal direction 2

Figure 5. Three-Component Micro-Vibration Time Histories and Corresponding Frequency Spectra at Monitoring Point 3.

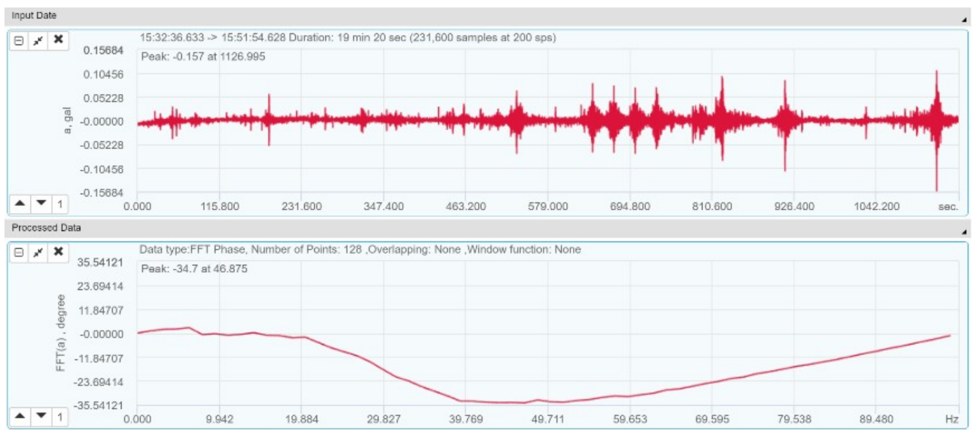

(a) Vertical direction

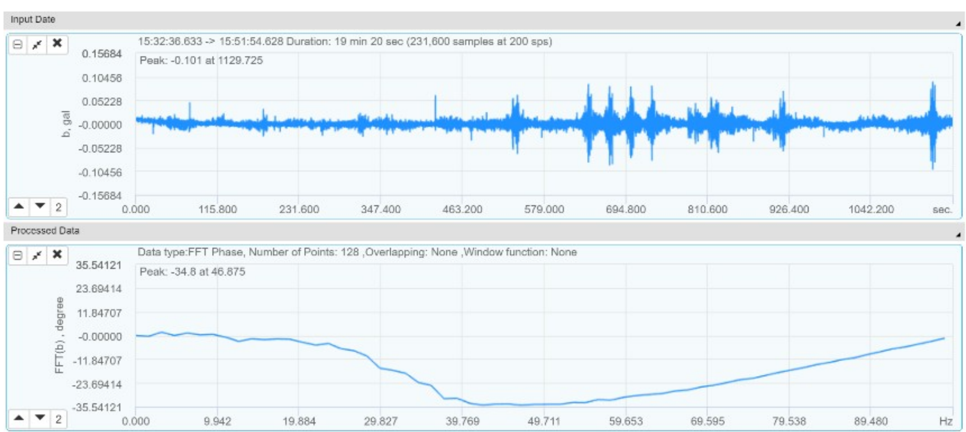

(b) Horizontal direction 1

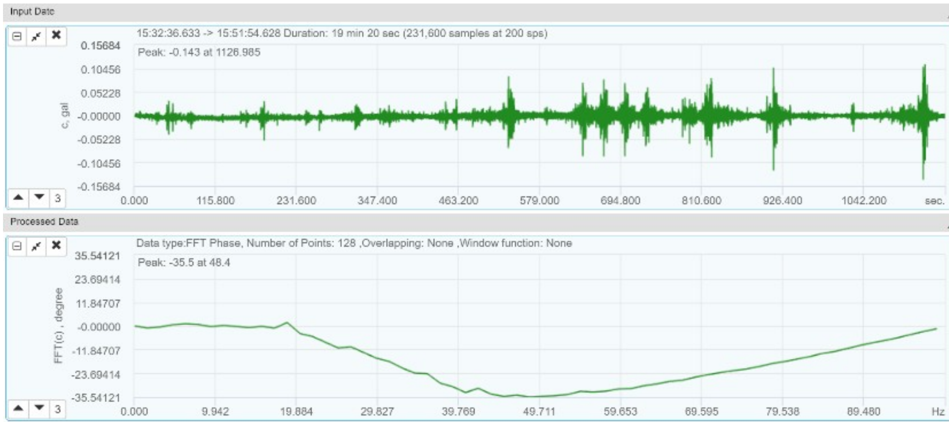

(c) Horizontal direction 2

Figure 6. Three-Component Micro-Vibration Time Histories and Corresponding Frequency Spectra at Monitoring Point 4.

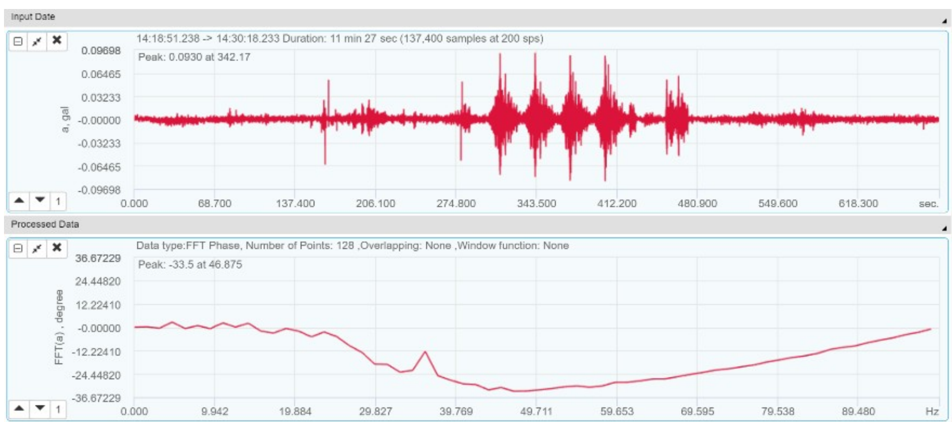

(a) Vertical direction

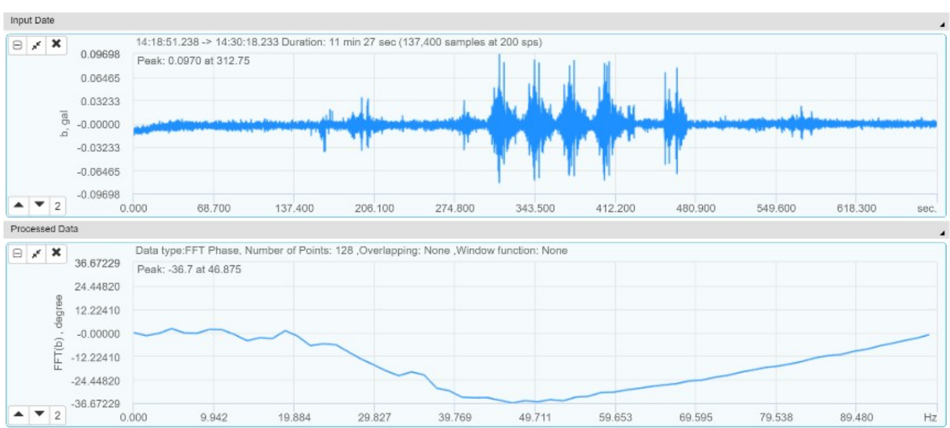

(b) Horizontal direction 1

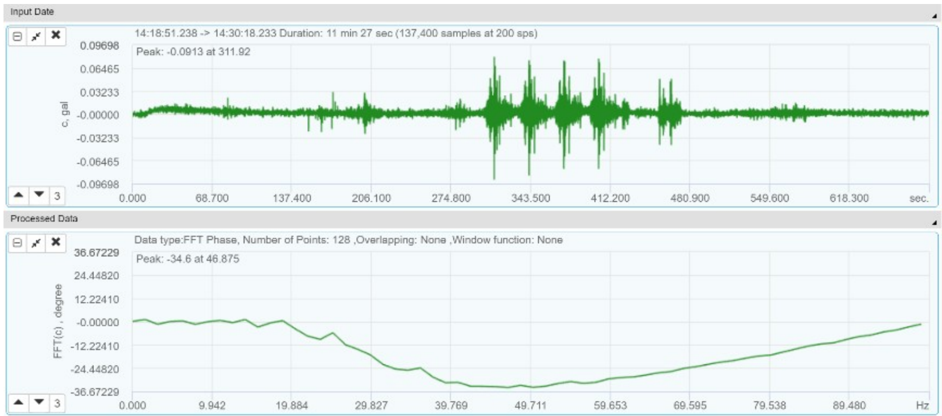

(c) Horizontal direction 2

Figure 7. Three-Component Micro-Vibration Time Histories and Corresponding Frequency Spectra at Monitoring Point 5.

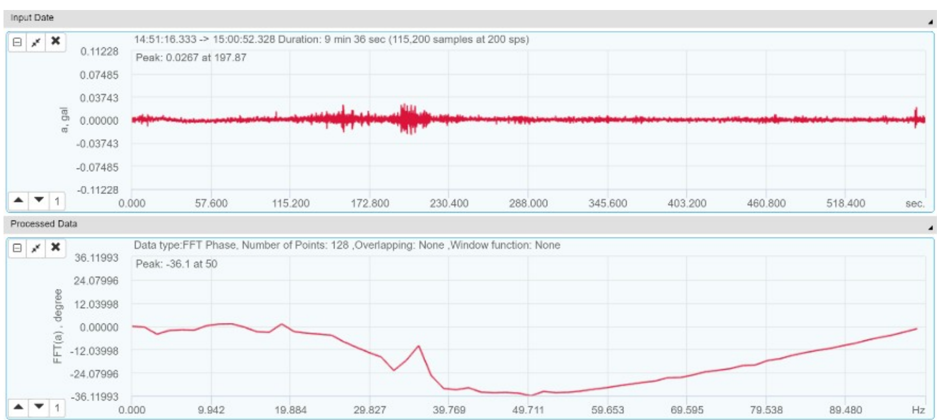

(a) Vertical direction

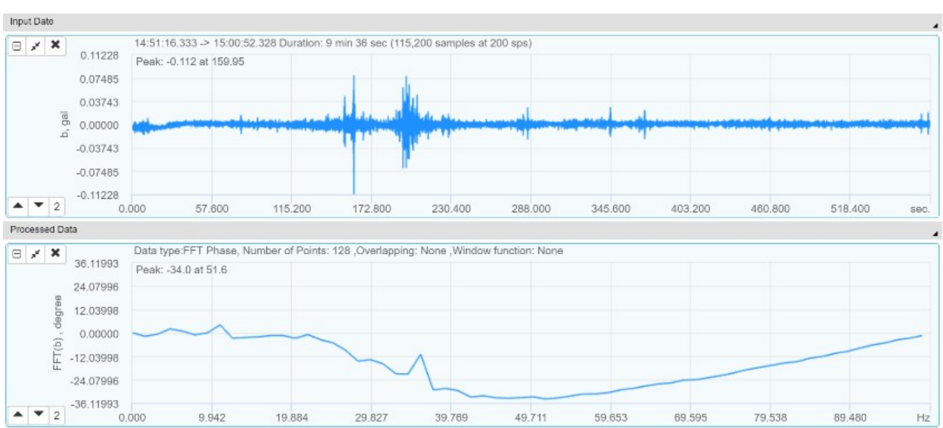

(b) Horizontal direction 1

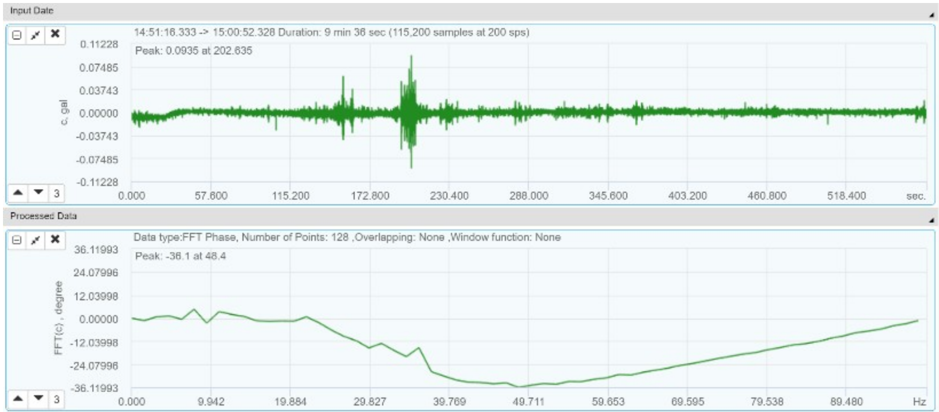

(c) Horizontal direction 2

Figure 8. Three-Component Micro-Vibration Time Histories and Corresponding Frequency Spectra at Monitoring Point 6.

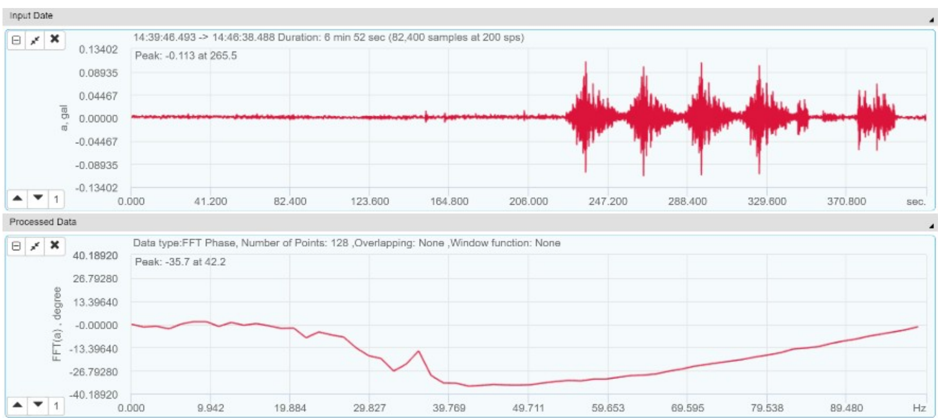

(a) Vertical direction

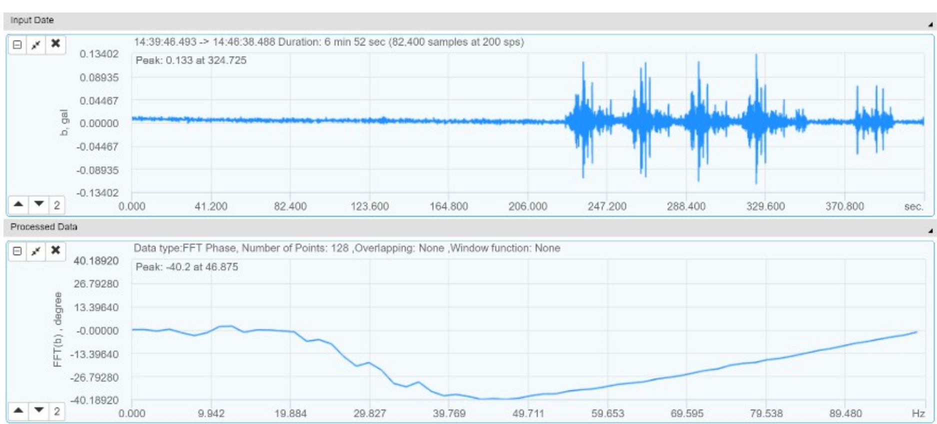

(b) Horizontal direction 1

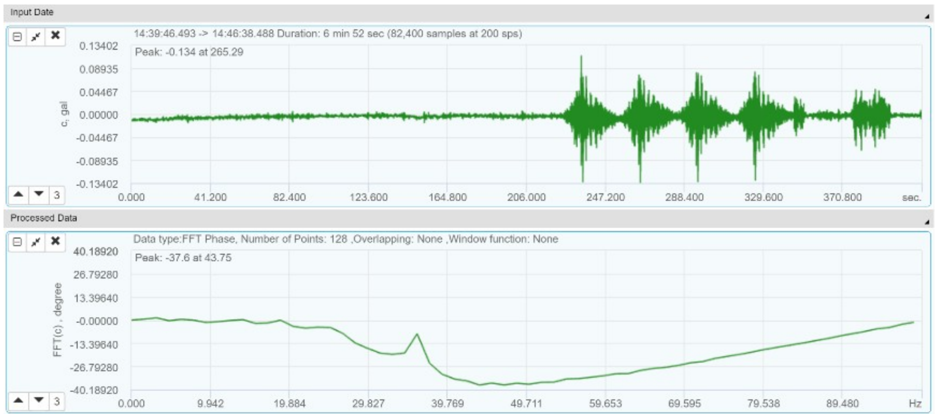

(c) Horizontal direction 2

Figure 9. Three-Component Micro-Vibration Time Histories and Corresponding Frequency Spectra at Monitoring Point 7.

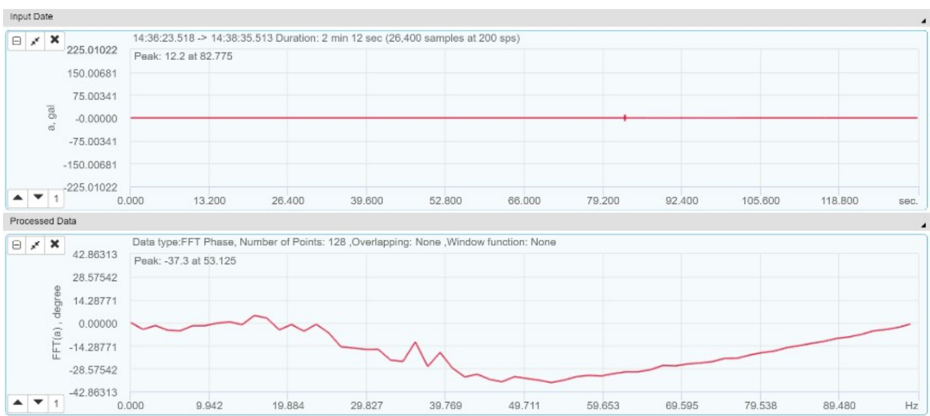

(a) Vertical direction

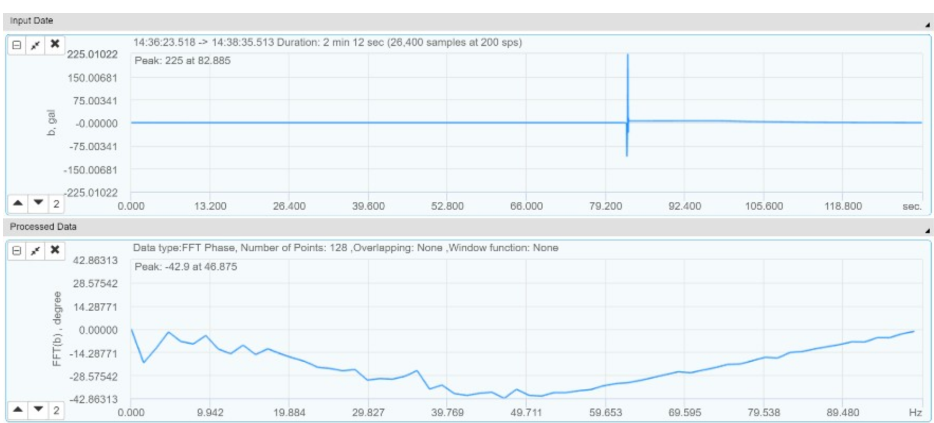

(b) Horizontal direction 1

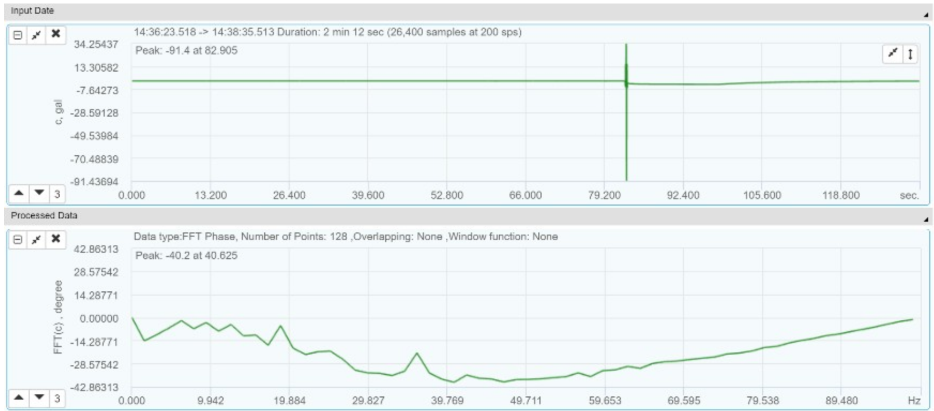

(c) Horizontal direction 2

Figure 10. Three-Component Micro-Vibration Time Histories and Corresponding Frequency Spectra at Monitoring Point 8.

Comparison and Discussion

For the area surrounding the collapsed school building at Guangfu Junior High School in Wufeng, Figures 3 through 10 present the spectral analysis results obtained from the microtremor acceleration time histories recorded at the eight monitoring points indicated in Figure 1.

Table 1 summarizes the maximum absolute spectral amplitudes and their corresponding frequencies in the vertical, horizontal-1, and horizontal-2 directions at each measurement point.

Table 1. Maximum absolute phase angles of the vertical component and corresponding frequencies at the eight measurement points.

No.	Vertical Direction	Horizontal 1 direction	Horizontal 2 direction
Point 1	-37.3° (43.75Hz)	-36.6° (39.1Hz)	-35.2°(40.625Hz)
Point 2	-37.0° (43.75Hz)	-41.0° (39.1Hz)	-41.3° (40.625Hz)
Point 3	-39.3° (42.2Hz)	-36.9°(40.625Hz)	-40.1° (42.2Hz)
Point 4	-34.7° (46.875Hz)	-34.8° (46.875Hz)	-35.5°(48.4Hz)
Point 5	-33.5° (46.875Hz)	-36.7° (46.875Hz)	-34.6° (46.875Hz)
Point 6	-36.1° (50.0Hz)	-34.0° (51.6Hz)	-36.1° (48.4Hz)
Point 7	-35.7°(42.2Hz)	-40.0° (46.875Hz)	-37.6° (43.75Hz)
Point 8	-37.3° (53.125Hz)	-42.9° (46.875Hz)	-40.2° (40.625Hz)

Comparison of the Maximum Absolute Phase Angles in Frequency Spectra

The micro-vibration acceleration time-series data recorded at the eight measurement points were analyzed using the Fast Fourier Transform (FFT) to obtain phase angle spectra, as depicted in Figures 2 through 9 (phase angles are represented on the vertical axis).

Table 1 summarizes the maximum absolute phase angles and their corresponding frequencies for all eight points. By comparing these maximum phase angles, phase angle deviations between each pair of measurement points can be evaluated. Additionally, frequency shifts are assessed by comparing the frequencies at which these maximum phase angles occur for each measurement direction.

The observed deviations in maximum absolute phase angles and their associated frequency shifts among pairs of points within the same direction are attributed to soil loosening induced by shear banding. This loosening effect reduces the soil's mass density, increases void space, and consequently alters the propagation velocity of micro-waves through the soil.

Table 2 details the relative phase angle shifts between each pair of points in the vertical, horizontal-1, and horizontal-2 directions, respectively:

1. Vertical direction: The minimum phase angle shift is 33.5° at Point 5, while the maximum shift of 39.3° occurs at Point 4, resulting in a maximum relative phase angle shift of 5.8°.

2. Horizontal-1 direction: The minimum phase angle shift is 34.0° at Point 6, and the maximum shift is 42.9° at Point 8, yielding a maximum relative phase angle shift of 8.9°.

3. Horizontal-2 direction: The minimum phase angle shift of 35.2° occurs at Point 1, whereas the maximum shift of 41.3° is observed at Point 2, corresponding to a maximum relative phase angle shift of 6.1°.

Table 2. Relative phase angle and frequency offsets among the eight measurement points.

	Relative offset of the phase angle and frequency of the spectrum		
	Vertical Direction	Horizontal Direction 1	Horizontal Direction 2
Point 1-Point 5	3.8° (3.125Hz)	4.3° (1.575Hz)	9.1° (10.95Hz)
Point 2-Point 5	3.5° (3.135Hz)	4.3°(7.775Hz)	6.7° (6.25Hz)
Point 3-Point 5	5.8° (4.675Hz)	0.2° (6.25Hz)	5.5°(1.525Hz)
Point 4-Point 5	1.2° (0.00Hz)	1.9° (0.00Hz)	0.9° (1.525Hz)
Point 6-Point 5	2.6° (3.125Hz)	2.7° (4.125Hz)	1.5° (1.525Hz)
Point 7-Point 5	2.2° (4.775Hz)	3.3° (0.00Hz)	3.0° (3.125Hz)
Point 8-Point 1	8.7° (12.5Hz)	3.5° (4.675Hz)	8.4° (14.075Hz)

Comparison of Relative Frequency Shifts

As shown in Table 5.2:

1. Vertical direction: The minimum frequency shift of 42.2 Hz occurs at Points 3 and 7. The maximum frequency shift is observed at Point 8 with a value of 53.125 Hz, yielding a maximum relative frequency shift of 12.5 Hz.

2. Horizontal-1 direction: The minimum frequency shift of 39.1 Hz is recorded at Points 1 and 2, while the maximum frequency shift of 51.6 Hz occurs at Point 6. This corresponds to a maximum relative frequency shift of 12.5 Hz.

3. Horizontal-2 direction: Points 1, 2, and 8 share the minimum frequency shift of 40.625 Hz. The maximum frequency shift of 48.4 Hz is observed at Points 4 and 6, resulting in a maximum relative frequency shift of 7.775 Hz.

Shear Banding Identification Based on Phase Angle Shifts

When two adjacent measurement points are located on opposite sides of a shear band, the relative phase angle offset between them is generally not significant. Therefore, to identify potential displacement of the shear zone between adjacent points, it is necessary first to assess the moderate displacement corresponding to the moderate damage degree of the building at the selected reference point, Point 5.

Based on this assessment, the relative phase angle offset δ between two measurement points is classified as follows:

1. Moderate displacement: $0 \le \delta \le 5°$
2. High displacement: $5° < \delta$

Using this criterion, the possible displacement of the shear zone between adjacent points can be estimated from the relative phase angle offsets among the eight measurement points, as presented in Table 3.

Table 3 summarizes the estimated levels of shear banding between adjacent measurement points based on these relative phase angle shifts.

Table 3. Shear banding level estimation using relative phase angle shifts at eight measurement points

	Vertical Direction	Horizontal Direction 1	Horizontal Direction 2
P1-P5	3.8° (medium level)	4.3°(medium level)	9.1°(medium level)
P2-P5	3.5° (medium level)	4.3°(medium level)	6.7°(high level)
P3-P5	5.8°(high level)	0.2° (medium level)	5.5°(high level)
P4-P5	1.2°(medium level)	1.9°(medium level)	0.9°° (medium level)
P6-P5	2.6°(medium level)	2.7°(medium level)	1.5°(medium level)
P7-P5	2.2°(medium level)	3.3°(medium level)	3.0°(medium level)
P8-P5	3.8°(medium level)	6.2°(high level)	5.6° (high level)

Determination of Shear Banding Levels Based on Frequency Shifts

When two adjacent measurement points are located within the shear zone simultaneously, the relative frequency offset between them is generally insignificant. Therefore, to identify the potential displacement of the shear zone between adjacent points, it is first necessary to evaluate the moderate displacement corresponding to the moderate building damage at the selected reference point, Point 5.

Based on this evaluation, the relative frequency offset Δ\DeltaΔ between two measurement points is classified as follows:

1. Moderate displacement: $0 \le \Delta \le 10$Hz
2. High displacement: $\Delta > 10$ Hz

Using these criteria, the possible displacement of the shear zone between adjacent points can be estimated from the relative frequency offsets among the eight measurement points, as summarized in Table 4.

Table 4. Estimation of Shear Banding Level Using Relative Frequency Shifts of Spectrum between Eight Measurement Points

	Vertical Direction	Horizontal Direction 1	Horizontal Direction 2
P1-P5	3.125Hz (medium level)	1.575Hz (medium level)	10.95Hz (high level)
P2-P5	3.135Hz (medium level)	7.775Hz (medium level)	6.25Hz (medium level)
P3-P5	4.675Hz (medium level)	6.25Hz (medium level)	1.525Hz (medium level)
P4-P5	0.00Hz (medium level)	0.00Hz (medium level)	1.525Hz (medium level)
P6-P5	3.125Hz (medium level)	4.125Hz (medium level)	1.525Hz (medium level)
P7-P5	4.775Hz (medium level)	0.00Hz (medium level)	3.125Hz (medium level)
P8-P5	6.25Hz (medium level)	0.00Hz (medium level)	6.25Hz (medium level)

Verification of Shear Banding Level

After determining the shear banding level in the three directions between each pair of adjacent measurement points using phase angle or frequency shifts, the maximum shear banding level is adopted as the representative level. Based on the results summarized in Table 5.4, the following conclusions can be drawn:

1. Moderate shear banding is observed between Points 4 and 5, Points 6 and 5, and Points 7 and 5.
2. Severe shear banding (Hsu, 1987; Hsu, 2022; Rice, 1976) occurs between Points 1 and 5, Points 2 and 5, Points 3 and 5, and Points 8 and 5.

During the 921 Jiji earthquake, as illustrated in Figures 1, 11, 12, 13, and 14, the ground near Points 1, 4, and 5 exhibited moderate shear banding levels, whereas the areas near Points 2, 3, 6, 7, and 8 experienced high shear banding levels. This observed distribution primarily resulted from significant shear banding in the first and second zones, which induced tilting and uplifting effects, as depicted in Figures 11 and 13.

Figures 11 to 14 further illustrate the shear banding effects, including the tilting and uplifting phenomena within the first and second zones.

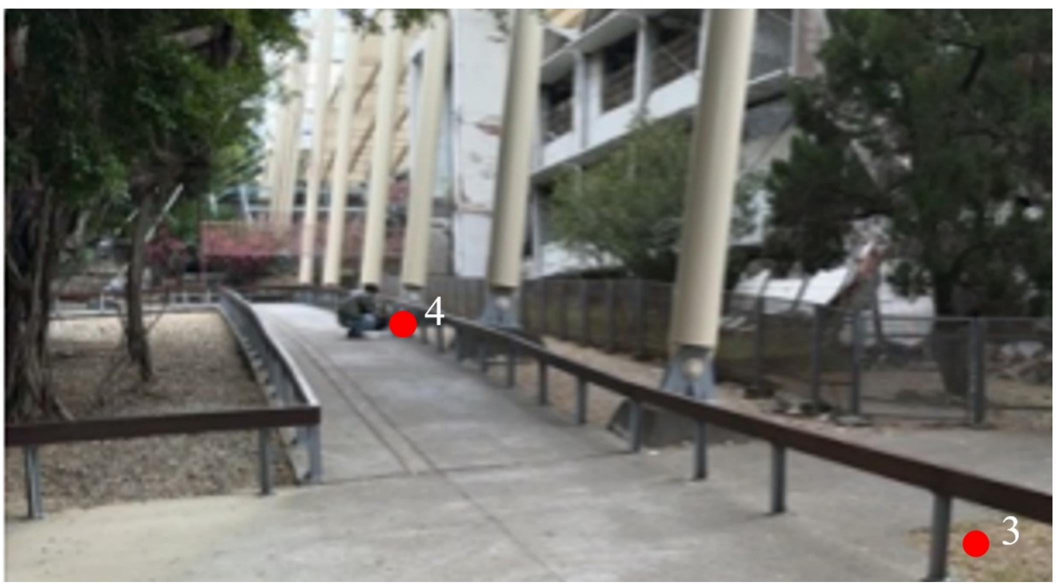

Figure 11. Slope deformation induced by first-stage shear band tilt and uplift.

Figure 12. The school building failure occurred in the first stage.

Figure 13. The second-stage shear-band tilted and uplifted slope (facing outside the school).

Figure 14. The school building collapsed during the second stage (facing the interior of the school).

The verification results indicate that the micro-vibration wave propagation acceleration time history data collected at each measurement point can be transformed into spectra using the Fast Fourier Transform (FFT). The phase angle shifts and corresponding frequency shifts between each pair of measurement points were employed to quantitatively evaluate the level of shear banding.

The quantitatively assessed shear banding levels were then compared with the actual shear bands observed in the school building during the 921 Jiji earthquake. It was found that, among the eight measurement points, the shear banding levels at Points 2 through 7 closely matched the observed levels. However, slight discrepancies were noted at Points 1 and 8: the quantitative assessment at Point 1 indicated a high shear banding level, whereas the actual shear banding was moderate; conversely, at Point 8, the quantitative assessment showed moderate shear banding, while the actual level was high.

These verification results demonstrate that evaluating shear banding levels using the relative offsets of spectral phase angles and frequency shifts between measurement points provides an accurate assessment.

Conclusions and Recommendations

The findings of this study support the following conclusions:

1. Shear banding is a primary cause of building failure during earthquakes.
2. Seismic design codes require a broader scope to address various failure mechanisms.
3. Building failures should be classified based on their predominant causes, including different levels of shear banding.
4. Existing seismic design codes (Construction and Planning Administration, Ministry of the Interior, 2015; International Building Code, 2021) have limitations.
5. Boundary conditions change from seismic to non-seismic scenarios, affecting structural responses.
6. A quantitative method for shear band identification enables classification of building vulnerability into non-seismic levels, categorized as mild, moderate, or high.

Based on these conclusions, three recommendations are proposed:

1. Update seismic design practices to incorporate shear banding and other non-seismic conditions.
2. Revise seismic design strategies to include a wider range of failure mechanisms, such as shear banding.
3. Promote future applications of quantitative shear band identification methods to enable objective assessment of a building's seismic vulnerability.

References

Construction and Planning Administration, Ministry of the Interior, Taiwan, *Building Technical Regulations*, 2015

Google Earth, Website: http://www.google.com.tw/intl/zh-TW/earth/, 2023

Hsu, Tse-Shan, Capturing Localizations in Geotechnical Failures, Ph.D. Dissertation, Civil Engineering in the School of Advanced Studies of Illinois of Technology, 1987.

Hsu, Tse-Shan, "Seismic Conditions Required to Cause Structural Failures in Tectonic Earthquakes," A Chapter in *Natural Hazards-New Insight*s, Edited by Mohammad Mokhtari, 2022

International Building Code (IBC), Version September, Website: https://codes.iccsafe.org/content/IBC2021P2, 2021

Rice, J. R., "The Localization of Plastic Deformation," in *Theoretical and Applied Mechanics, Proceedings of the 14th International Congress on Theoretical and Applied Mechanics*, Delft, 1976, ed. W.T. Koiter, North Holland, Amsterdam, Vol. 1, pp. 207-220, 1976

Wen, Y. E "Research on Micro Vibration Measurement and Analysis Method of Using," *Metrology Science and Technology*, Vol. 67, No. 6, pp. 44-48, 2023